Nanoscale

PAPER

View Article Online
View Journal | View Issue

Check for updates

Cite this: *Nanoscale*, 2017, **9**, 7179

Surface passivation and self-regulated shell growth in selective area-grown GaN–(Al,Ga)N core–shell nanowires†

Martin Hetzl, *[a] Julia Winnerl,[a] Luca Francaviglia, [b] Max Kraut,[a] Markus Döblinger,[c] Sonja Matich,[a] Anna Fontcuberta i Morral[b] and Martin Stutzmann[a]

Received 3rd February 2017,
Accepted 7th May 2017

DOI: 10.1039/c7nr00802c

rsc.li/nanoscale

The large surface-to-volume ratio of GaN nanowires implicates sensitivity of the optical and electrical properties of the nanowires to their surroundings. The implementation of an (Al,Ga)N shell with a larger band gap around the GaN nanowire core is a promising geometry to seal the GaN surface. We investigate the luminescence and structural properties of selective area-grown GaN–(Al,Ga)N core–shell nanowires grown on Si and diamond substrates. While the (Al,Ga)N shell allows a suppression of yellow defect luminescence from the GaN core, an overall intensity loss due to Si-related defects at the GaN/(Al,Ga)N interface has been observed in the case of Si substrates. Scanning transmission electron microscopy measurements indicate a superior crystal quality of the (Al,Ga)N shell along the nanowire side facets compared to the (Al,Ga)N cap at the top facet. A nucleation study of the (Al,Ga)N shell reveals a pronounced bowing of the nanowires along the *c*-direction after a short deposition time which disappears for longer growth times. This is assigned to an initially inhomogeneous shell nucleation. A detailed study of the proceeding shell growth allows the formulation of a strain-driven self-regulating (Al,Ga)N shell nucleation model.

1. Introduction

The fabrication of coaxial core–shell nanowire (NW) heterostructures has moved into focus of research thanks to new applications and benefits compared to plain NWs consisting of only one material. In the case of nitride-based NW structures, core–shell NW growth is used, *e.g.*, for nonpolar quantum well structures, which are promising to improve the optical performance of light-emitting diodes, and also for ultraviolet photodetection.[1–3] Moreover, in a recent publication, we have demonstrated the controlled strain-induced tuning of the GaN NW band gap toward higher energies with the help of an (Al,Ga)N shell.[4] However, in particular for core–shell structures with comparably thick shells (>30 nm), where strain effects play a major role, the nucleation mechanism of the shell and defects within the heterostructures are scarcely investigated. Hence, the nanoscale optical and structural properties of heteroepitaxial selectively grown GaN–(Al,Ga)N core–shell NWs are presented in this work. First, an overview of macroscopic photoluminescence (PL) properties for distinct core–shell NW geometries on Si substrates is discussed and compared with core–shell NWs grown on diamond substrates. Then, we turn our attention to the optical and structural characteristics on the nanoscale. In particular, cathodoluminescence (CL) measurements of pure GaN NWs are compared with different GaN–(Al,Ga)N core–shell NWs and provide a spatially resolved insight into the different luminescence properties of both the GaN core and the (Al,Ga)N shell. The origin of defect emissions are further addressed by scanning transmission electron microscopy (STEM) with special emphasis on the (Al,Ga)N shell. To understand the growth process of the shell, a series of GaN–(Al,Ga)N core–shell NWs with varying deposition time of the shell has been fabricated. A scanning electron microscopy (SEM) study in combination with cross-sectional transmission electron microscopy (TEM) allows the reconstruction of the shell nucleation process and the proposal of a strain-driven self-regulating nucleation model.

[a]*Walter Schottky Institut and Physics Department, Technische Universität München, 85748 Garching, Germany. E-mail: martin.hetzl@wsi.tum.de, stutz@wsi.tum.de*
[b]*Laboratoire des Matériaux Semiconducteurs, École Polytechnique Fédérale de Lausanne, 1015 Lausanne, Switzerland*
[c]*Department of Chemistry, Ludwig-Maximilians-Universität München, 81377 Munich, Germany*

†Electronic supplementary information (ESI) available: Numerical simulations of the electron density in GaN–(Al,Ga)N core–shell nanowires. Wavelength-dependent CL detection. CL spectra of GaN and GaN–(Al,Ga)N core–shell nanowires on Si at distinct sites with no vertical shift. CL spectra of GaN–(Al,Ga)N core–shell nanowires on diamond. Electron dispersive X-ray spectroscopy of a GaN–(Al,Ga)N core–shell NW. TEM images of GaN–(Al,Ga)N core–shell nanowires with a thicker core diameter. CL analysis of a GaN–(Al,Ga)N core–shell NW with a thin shell. See DOI: 10.1039/C7NR00802C

2. Experimental

The core–shell NWs in this work have been grown by means of plasma-assisted molecular beam heteroepitaxy on Si (111) and on diamond (111) in a selective area growth (SAG) approach. To this end, a 10 nm thin Ti film has been evaporated directly on the substrate.[5–7] Then, arrays of holes defining the nucleation sites of the NWs have been established with different diameters and periods into the Ti by e-beam lithography and wet chemical etching. This allows a controlled variation of the GaN NW core on the same substrate to obtain a maximum of information from a single growth cycle. In this particular work, the GaN cores have been grown for 90′ under highly N-rich conditions at a substrate temperature of 850 °C yielding a NW length of ≈600 nm and diameters ranging from 40 to 155 nm on Si substrate and 130 to 240 nm on diamond. In addition, the period has been varied from 300 to 2000 nm. Directly after the GaN core growth, Al has been supplied as well to achieve an Al content of nominally 95% within the (Al,Ga)N shell. Note that the Al content has been obtained from (Al,Ga)N reference layers measured by high-resolution X-ray diffraction. To enhance lateral growth at the NW side facets the substrate temperature has been decreased by 20 K for the shell growth, leading to a maximum shell thickness of 50 nm after 30′ growth time. A detailed description of GaN–(Al,Ga)N core–shell NW SAG can be found in a previous publication.[4]

The measurement setups and the corresponding parameters for μ-PL, CL and STEM are equivalent to those in ref. 4. TEM, applied for the shell nucleation study, has been performed with a FEI Tecnai transmission electron microscope at an acceleration voltage of 200 kV. To achieve electron transparency, the core–shell NWs have been released from their original substrate and dispersed on a copper grid covered with a holey carbon film.

3. Results and discussion

In Fig. 1 selected room temperature PL spectra near the band edge are plotted for different GaN–(Al,Ga)N core–shell NW structures grown on Si and diamond substrates. All spectra have been recorded on as-grown NWs with an incident laser beam parallel to the NW growth axis and a spot size of several micrometers, which results in an excitation of an ensemble of NWs. In the case of bare GaN NWs and core–shell NWs after 30′ shell growth, tilted view SEM images are attached to the diagram. While the bare GaN NWs are free-standing on their original site, parasitic (Al,Ga)N nucleation occurs in the case of core–shell NWs. This has been addressed in detail in a previous publication.[4] A main characteristic for different (Al,Ga)N shell thicknesses is the energetic variation of the PL peak centers of the GaN core, which has been assigned to compressive strain within the GaN core along its growth direction.[4,8–11]

A phenomenon which has not been addressed so far is the loss of PL intensity of the NWs grown on Si once coated with the (Al,Ga)N shell. In particular, a decrease of the PL intensity

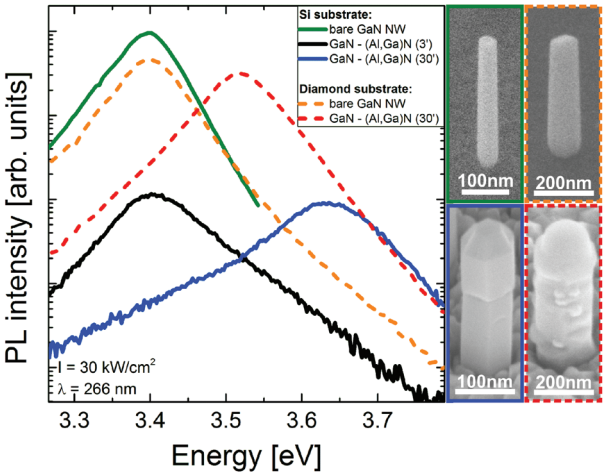

Fig. 1 Selection of room temperature PL spectra for specific core–shell NW arrays on Si and diamond substrates. The growth time of the (Al,Ga)N shell is indicated by brackets in the legend. *I* and λ are the excitation intensity and the wavelength of the PL laser, respectively. Tilted view SEM images (45°) of bare GaN NWs and core–shell NWs with 30′ of shell growth are attached to the diagram. The colored frames of the SEM images correlate with the respective colors of the PL spectra.

of core–shell NWs with t_{shell} = 30′ (blue curve) by two orders of magnitude with respect to the bare GaN NWs (green curve) can be identified. Possible reasons for this intensity loss are: (i) defect absorption within the (Al,Ga)N bulk; (ii) decreased in- and outcoupling efficiency of light; (iii) nonradiative recombination centers at the GaN/(Al,Ga)N interface; (iv) spatial charge carrier separation within the core due to band bending at the core–shell interface.

Firstly, defects in the (Al,Ga)N shell or the cap might absorb both the laser light and the GaN emission. This, in turn, would attenuate the GaN signal measured by PL. Due to the preferred growth in *c*-direction, a pronounced (Al,Ga)N cap with a height of ≈250 nm is present for these NWs, whereas the shell has a much lower thickness of 50 nm. To clarify this influence, the PL spectrum of an equivalent NW array with a shorter t_{shell} = 3′ is plotted in Fig. 1 (black curve). Despite a smaller (Al,Ga)N cap with a height of ≈20 nm the peak intensity is similar to the NWs with a thick cap. Consequently, defect absorption within the bulk of the (Al,Ga)N can be ruled out as a main issue for the decreased PL intensity of core–shell NWs on Si. Note that apart from the expected energy shift towards the GaN band gap, a pronounced tail on the high energy side for the 3′ shell indicates inhomogeneities in the shell nucleation after this short growth time. This will be further discussed in the structural analysis part of this work.

A higher reflection coefficient of the incident laser light at the top facet can also be excluded as an origin for the intensity drop: assuming a refractive index of n = 2.34 at λ = 266 nm (for AlN),[12] this results in a reflectivity at the top facet of only 16% according to Fresnel's law. In addition, measurements on released NWs with PL excitation over the side facets exclude a possible preferred outcoupling of emitted light over the sidewalls in the case of core–shell NWs.

The remaining reasons for the intensity decrease are nonradiative recombination channels originating from the GaN/(Al,Ga)N interface or/and charge carrier separation. Lefebvre *et al.* have reported a strong influence on the PL intensity of bare GaN NWs under different atmospheres.[13] In particular, oxygen (O) is known to be responsible for Fermi level pinning at the NW sidewalls and a resulting decrease in the radiative recombination efficiency.[14,15] Thus, impurities at the GaN/(Al,Ga)N interface might act as efficient nonradiative recombination centers. It seems natural that either O, Si or Ti from the Si substrate or the TiN mask are possible candidates for these kind of defects. O is a typical impurity in AlN even for highly pure crystals,[16] whereas Si is known to interdiffuse from the substrate into the onsets of GaN NWs causing unintentional n-type doping.[17] To elucidate this, equivalent GaN–(Al,Ga)N core–shell NWs have been grown on single crystalline diamond (111) substrates. From earlier publications it is known that GaN NWs on diamond are superior to those on Si substrate with respect to their optical properties.[18,19] One reason for this is the reduction of unintentional impurities from the substrate due to the high thermal, chemical and physical stability of diamond.[20] The growth parameters applied for NWs on diamond are equivalent to those on Si substrate. However, GaN NW growth on diamond is characterized by a slightly thicker diameter of the NWs compared to NWs on Si due to an enhanced lateral growth (SEM images in Fig. 1). A detailed comparison of bare GaN NWs on both substrates can be found in ref. 19. In contrast to the pronounced intensity quenching for core–shell NWs on Si, the PL intensities of bare GaN NWs and core–shell NWs on diamond are similar to each other (Fig. 1 dashed lines). In particular, the peak intensity of the core–shell NWs is about 70% of bare GaN NWs. This value is within the range of possible measurement uncertainties, *e.g.*, focus, excitation volume and fluctuations of the laser. Note that this trend has been observed for all core diameters, *i.e.* from 40 to 155 nm and 130 to 240 nm for NWs on Si and diamond, respectively. Consequently, the PL intensity quenching observed for core–shell NWs grown on Si does not occur on diamond and, thus, seems to be a substrate-specific effect. Worth mentioning is that the observed intensity quenching in the GaN core due to the (Al,Ga)N shell growth is reversible: after removing the shell by a potassium hydroxide bath the original intensity could be retrieved (not shown). This proves that the GaN core has not been damaged by the shell growth, ruling out this to be a reason for the measured intensity loss in PL. Ti and O can also be excluded as impurities causing the intensity decrease since TiN masks are implemented equivalently and the same (Al,Ga)N shell growth has been applied on both substrates. A doping effect due to interdiffusing Si into the NWs is also not the reason, since this would already affect the intensity for bare GaN NWs on Si substrate. Moreover, band bending in the GaN core due to unintentional Si doping of both the (Al,Ga)N shell and the GaN core is unlikely to be the reason. Numerical simulations of the band structure have shown that despite a more pronounced band bending toward the interface for higher doping, enough charge carriers are present to allow a direct recombination (ESI†). Thus, we assume Si-related defect centers at the GaN/(Al,Ga)N interface to be responsible for the observed reduction of the radiative recombination efficiency of heteroepitaxial GaN–(Al,Ga)N core–shell NWs on Si. These defects might either act as nonradiative recombination paths or induce a band bending which separates electrons and holes and reduces thus the recombination efficiency. Note that the intensity quenching for core–shell NWs on Si compared to diamond substrates does not correlate with the shell surface morphology. In contrast, core–shell NWs on Si show a smoother surface than NWs on diamond (SEM images in Fig. 1).

In order to obtain more information about the origin of nonradiative defect centers in core–shell NWs, power-dependent PL measurements have been performed on GaN–(Al,Ga)N core–shell NWs on both substrates. In particular, the GaN–(Al,Ga)N core–shell NWs with a 30′ grown shell from Fig. 1 have been investigated. The resulting integrated PL intensities (Fig. 2a) have been fitted with the expression $I_{PL} \propto (I_{Exc})^{\alpha}$, with I_{PL} the integrated PL intensity, I_{Exc} the excitation density of the laser and α the slope in the double logarithmic scale. For core–shell NWs on Si, a superlinear dependence with α = 1.2 has been obtained over the whole measurement range, whereas for core–shell NWs on diamond, a linear increase (α = 1.0) until 0.35 kW cm^{-2} has been identified, followed by a superlinear increase of α = 1.5 for higher excitation densities. Similar trends have been obtained for all NW diameters. A superlinear increase of the PL intensity can have various origins, namely different recombination mechanisms, *e.g.* excitonic or free carrier recombination,[21] different emission regimes, *e.g.* spontaneous emission or amplified spontaneous emission (ASE),[22] or defect saturation.[23] To clarify this for the particular case, the corresponding full-width-at-half-maximums (FWHMs) are plotted in Fig. 2b as a function of the excitation density. In the case of core–shell NWs on diamond, a distinct decrease of the FWHM from ≈105 to 60 meV can be observed for excitation densities higher than 0.35 kW cm^{-2}. Obviously, the increase in α (Fig. 2a) correlates with the decrease of the FWHM (Fig. 2b). This phenomenon is characteristic for the transition from spontaneous emission to ASE, which has been also observed

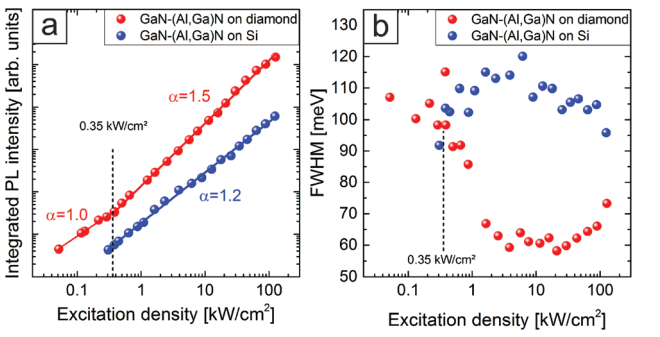

Fig. 2 (a) Integrated PL intensity of SAG GaN–(Al,Ga)N core–shell NWs on Si and on diamond substrates as a function of the excitation density and (b) corresponding FWHMs.

for pure SAG GaN NWs in a similar excitation regime.[19] In contrast, core–shell NWs on Si show an unaltered FWHM for all excitation powers which is, in addition, on the same level like the FWHM of core–shell NWs on diamond in the case of low excitation densities. Thus, we assume that the PL emission from core–shell NWs on Si is spontaneous emission, whereas its superlinear slope is due to nonradiative defect saturation.

Worth mentioning is a blueshift of 5 meV with increasing excitation density for core–shell NWs on diamond which indicates band filling (not shown). This is in agreement with the observed increase of the FWHM for excitation densities higher than 20 kW cm^{-2} due to power broadening. In contrast, on Si substrates, the opposite trend has been observed, *i.e.* a redshift by 5 meV. This might be explained by a significant heating of the sample due to the excitation of the Si substrate beneath, whereas the diamond substrate is transparent for the excitation wavelength. Thus, based on the distinctively different impact of the respective substrate species on the PL measurements, an irrevocable correlation of the power-dependent PL intensity evolution and defect saturation is challenging in the present case.

In order to investigate defects within a NW without disturbing influences of the substrate and to clarify the influence of the shell morphology on the optical properties of core–shell NWs, measurements on the nanoscale are necessary. In the following NWs with different core–shell specifications are investigated by SEM-CL. Due to the strongly localized excitation volume in CL (spot size <10 nm) compared to PL (spot size >1 μm), CL allows to reach very high local densities of excitation energy. Thanks to the small interaction volume, the overall excess heat is dissipated in the surrounding NW volume with no major damages to the semiconductor.

In Fig. 3a and b, CL spectra of selected sites, false-colored CL maps and corresponding SEM images are displayed in the case of a bare GaN NW and a GaN–(Al,Ga)N core–shell NW on Si, respectively. "Green" in the CL maps corresponds to the intensity at an energy of 3.44 eV for the bare GaN NW and 3.67 eV for the core–shell NW, whereas "red" is related to an emission at 3.25 eV. In the case of a bare GaN NW (Fig. 3a) a homogeneous CL signal over the whole NW cross section has been observed. In particular, two different emission lines, a sharp peak at 3.44 eV and a broader peak at 2.18 eV have been assigned to the band gap recombination of free A-excitons (X_A) and the well-known yellow luminescence (YL) of GaN, respectively.[24–26] The small peak at 1.72 eV represents the second harmonic of the X_A emission. The peak intensities of YL and X_A are in the same order of magnitude. In the literature, YL has been assigned to a donor–acceptor-pair recombination process (DAP) where point defects such as Ga vacancies or carbon impurities act as deep acceptors.[25,27] Thus, the pronounced YL emission is an indication for a significant density of point defects in SAG GaN NWs on Si. However, it should be mentioned that the CL setup used is optimized to a spectral energy around 2.5 eV, which leads to an overestimation of YL compared to X_A by a factor of three to four (ESI†). Note that the YL signal is distinctively lower for self-assembled GaN NWs on Si and seems, thus, to be a growth mode specific effect (ESI†).

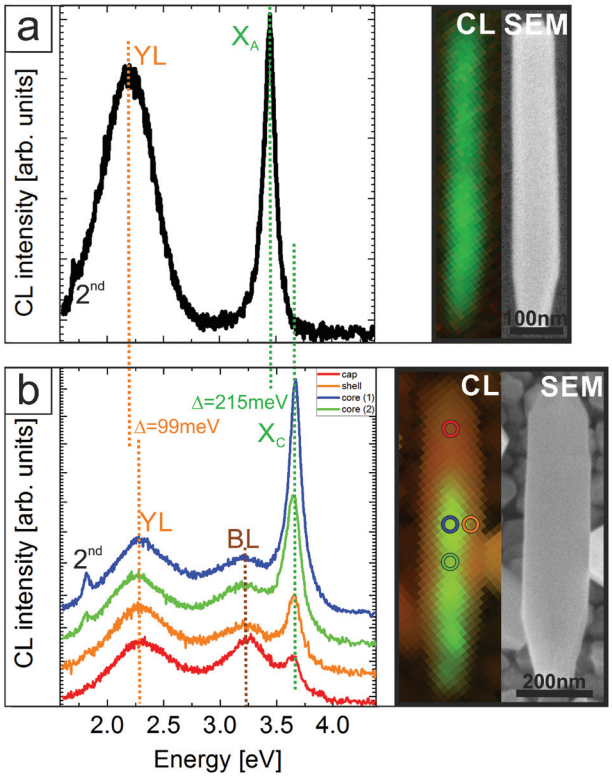

Fig. 3 Room temperature CL spectra of (a) a bare SAG GaN NW on Si with a diameter of 81 nm and (b) distinct sites along a SAG GaN–(Al,Ga)N core–shell NW with a core diameter of 69 nm and a shell thickness of 46 nm with respective false-colored CL maps and SEM images. "Green" in the CL maps corresponds to the excitonic peak center, whereas "red" belongs to the BL emission. The colored circles in the CL map in (b) indicate the positions of the respective spectra.

In Fig. 3b, CL spectra of different locations along a GaN–(Al,Ga)N core–shell NW are displayed. The plotted spectra are vertically shifted with respect to each other for a better comparison. The corresponding raw data are given in the ESI.† The most pronounced signal has been measured at the upper part of the core (marked with a blue circle) with a sharp peak at 3.67 eV (X_C) and two broad emissions around 2.28 eV (YL) and 3.21 eV (blue luminescence, "BL"). Again, the small peak at 1.84 eV is related to the second harmonic of X_C. Equivalent to the X_A luminescence for bare GaN, the X_C emission is assigned to the band gap recombination of GaN and is blueshifted by 215 meV for this particular core–shell NW. Reason for this blueshift is, similar to the PL measurements (Fig. 1e), compressive strain within the GaN core which leads to a potential shift and a change of the energetically highest valence band from A-exciton to C-exciton.[4,9,10] In contrast, the energetic shift of the YL emission is 99 meV with respect to the bare GaN and is, thus, less pronounced than the band gap shift. Since the donor band for the DAP recombination of YL is similar to the conduction band of GaN (at room temperature),[28] the smaller strain-induced shift implies a discrepancy

in the deformation potentials of the unknown deep acceptor band and the GaN valence bands. Thus, a controlled variation of the strain could provide a better understanding of the properties of this ubiquitous defect in GaN.

At a slightly different location within the core (Fig. 3b, green circle), the overall intensity decreases to 60% of its original value and shifts to slightly lower energies ($\Delta E = -21$ meV). In agreement with the previous findings, the YL emission shows a less pronounced shift of ≈−14 meV which indicates strain fluctuations along the NW longitudinal axis as the origin for this energy shift. However, this fluctuation turns out to be a local phenomenon since the CL intensity increases again at lower regions of the NW, including a shift of the emission back to its previous value. An explanation has been given in ref. 4, where several nanometers deep cracks within the shell have been attributed to a variation of the local strain. In this work, another possible reason will be presented in the structural analysis section.

Apart from the GaN core, a CL spectrum of the core/shell interface is also included in Fig. 3b (orange curve). Naturally, the X_C luminescence decreases due to the decrease of GaN material in this region. Also the BL emission shows a slight attenuation. However, the YL emission is similar to the spectra obtained at the inner GaN core, which is an indication that YL is predominantly emitted in the vicinity of the GaN surface. This has also been reported by Li *et al.* who have measured CL on MOCVD-grown GaN NWs.[29] The relative decrease of the intensity ratio YL/X_C for core–shell NWs compared to YL/X_A for bare GaN NWs (Fig. 3a and b) by almost a factor of three indicates an attenuation of this defect thanks to the (Al,Ga)N shell.

In the case of the (Al,Ga)N cap (Fig. 3b, red curve), the BL emission becomes more prominent, accompanied by a blueshift from 3.21 to 3.25 eV. In the literature, the BL emission has been attributed to O impurities substituting N atoms (O_N). In combination with a triple negatively charged vacancy at an Al lattice site (V_{Al}^{3-}) a complex is formed acting as a DAP state.[16,30,31] In addition, it has also been shown that Si impurities enhance the BL signal in (Al,Ga)N thin films due to a lowering of the formation energy of V_{Al}^{3-}.[32,33]

To verify this, CL spectra of the GaN core of GaN–(Al,Ga)N core–shell NWs grown on Si and diamond substrates are plotted in Fig. 4. The spectra have been normalized on the X_C emission for a better comparison. The corresponding CL maps of the core–shell NW on diamond and spectra of different positions are discussed in the ESI.† Due to different core diameters on the respective substrates, the X_C emissions are, similar to the PL measurements (Fig. 2), energetically shifted to each other. However, the most prominent difference between both spectra is the absence of the BL emission peak in the case of the core–shell NW on diamond substrate. Note that the increased YL in the case of diamond substrates can be attributed to a significant luminescence contribution of point defects located within the diamond substrate (ESI†).

Thus, we expect that Si atoms, provided from the substrate during growth, diffuse along the NWs and are incorporated in the (Al,Ga)N which leads to the pronounced BL emission in

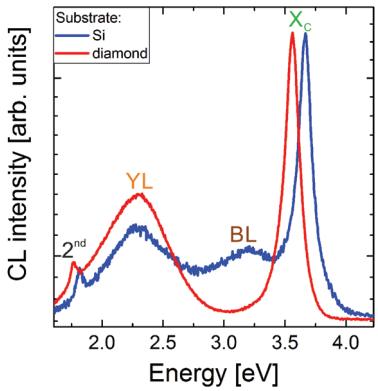

Fig. 4 CL spectra of the GaN core emission in GaN–(Al,Ga)N core–shell NWs grown on Si and diamond substrates.

the case of Si substrates. This incorporation seems to preferentially occur in the (Al,Ga)N cap, which leads to a local increase of V_{Al}^{3-} centers and, consequently, to an enhancement of the BL emission in this region. Worth mentioning is that both the X_C and the YL emissions are attenuated but still visible in the (Al,Ga)N cap (Fig. 3b). In the literature, there are no reports of YL emission for (Al,Ga)N alloys with a high molar fraction of Al. Thus, we expect that YL is indeed emitted from the GaN. In CL spectroscopy, the band gap of the (Al,Ga)N is also excited. Consequently, possible reasons for the detection of YL and X_C during excitation of the cap are: (i) GaN clusters within the (Al,Ga)N cap, (ii) diffusion of generated charge carriers from the (Al,Ga)N cap and recombination at the GaN/(Al,Ga)N interface; (iii) absorption and re-emission of light from the (Al,Ga)N shell at the GaN/(Al,Ga)N interface. Electron dispersive X-ray spectroscopy measurements on a core–shell NW exclude the presence of GaN inclusions within the cap (ESI†). Charge carrier diffusion is also unlikely to be the reason, as no diffusion length induced decrease of the YL emission has been observed during cap excitation for higher distances away from the GaN/(Al,Ga)N interface. Thus, absorption of emitted light from the (Al,Ga)N seems to be the reason for this observation. Note that the band gap excitation of (Al,Ga)N at around 6 eV could not be measured with the CL setup used as this energy regime is out of the detection range of the spectrometer.

In contrast to the PL measurements in Fig. 1, where the PL intensity of the band gap luminescence is attenuated by two orders of magnitude from bare GaN to core–shell NWs on Si, the CL intensity of X_C of the core–shell NW (Fig. 3b) exceeds the intensity of the X_A emission of the bare GaN NW (Fig. 3a) by a factor of ≈1.5 despite a slightly smaller core diameter. Henley *et al.* have shown for (In,Ga)N/GaN quantum well structures that for high CL excitation powers a saturation of non-radiative recombination centers can occur.[34] Transferred to our observations all CL spectra are blueshifted compared to the respective PL spectra by 20–40 meV, which can be assigned to band filling caused by the high electron excitation power of the CL setup.[35] Thus, the absence of an intensity drop in the

case of CL measurements from bare GaN to core–shell NWs is believed to result from an effective saturation of the Si-related defect centers located at the GaN/(Al,Ga)N interface which has already been suggested by power-dependent PL measurements (Fig. 2).

To address a possible correlation of defect emission and strain within the core–shell NWs, a cone-shaped NW has been investigated by CL. These type of NWs appear for core–shell SAG with a small period due to shadowing of next neighbor NWs during shell growth.[4] Note that the GaN core diameter is constant over the full length of these NWs. In particular, a cone-shaped SAG GaN–(Al,Ga)N core–shell NW with a core diameter of 120 nm and t_{shell} = 30′ released from an array of 300 nm period is investigated. In Fig. 5, CL spectra near the band edge at different sites, a corresponding false-colored CL map and a SEM image for this NW are depicted. "Blue" color in the CL map corresponds to the intensity at a photon energy of 3.61 eV, whereas "green" and "red" refer to 3.52 and 3.21 eV, respectively. Similar to the core–shell NW in Fig. 3b, a pronounced BL emission from the (Al,Ga)N cap has been detected (not shown in the spectra) which indicates a reduced crystal quality in this region. Naturally, due to the decrease of the shell thickness and, thus, a reduction of the strain, the peak energy of the GaN core (X_C) shifts to lower energies toward the NW bottom. In addition, also the X_C intensity decreases, whereas the YL and BL defect emissions from the GaN core surface and the (Al,Ga)N shell, respectively, remain constant. Thus, the GaN core emission intensity is influenced by the strain environment within a core–shell NW, whereas the defect emissions are not affected. As CL measurements on NWs with constant shell thicknesses have shown a uniform X_C luminescence along the whole NW (Fig. 3b), the non-isotropic strain degradation toward the NW bottom seems to be the reason for the intensity decrease in the cone-shaped NW and also the local intensity fluctuations observed in Fig. 3b. Note that an open GaN facet located at the NW onset due to the releasing of the NW from its original nucleation site could also contribute to the observed redshift toward the NW bottom. However, it has been shown in a previous work that this type of strain relaxation is very locally confined at the actual cleave edge, which excludes this to be the main reason for the observed energy and intensity gradients along the whole core–shell NW.[4]

The CL measurements described above have allowed a spatially resolved determination of radiative centers and fluctuations of the (Al,Ga)N shell and the strained GaN core. In the following, these emission characteristics are correlated with the crystal structure of the NWs. In particular, STEM measurements have been conducted on a GaN–(Al,Ga)N core–shell NW thinned from both sides by a focused ion beam (FIB) to achieve electron transparency.

In Fig. 6a, a cross-sectional TEM image of a core–shell NW grown on Si with a core diameter of 120 nm, a shell thickness of 50 nm and an (Al,Ga)N cap height of 250 nm is depicted. Distinct differences in the crystal structure between the (Al,Ga)N shell and the cap can be identified. In particular, the cap seems to grow as an extended crystal, whereas the shell is characterized by a crystallite growth perpendicular to the NW axis. Nevertheless, as these crystallites are completely merged with each other a closed shell layer with a homogeneous thickness can still be achieved. Thus, we can conclude that (Al,Ga)N with a high molar fraction of Al shows a crystallite growth behavior on the *m*-planes of a GaN NW, whereas on the *c*-plane the growth occurs preferentially single crystalline.

To obtain a more detailed insight into the crystal quality, high-angle annular dark field (HAADF) STEM has been performed at the GaN/(Al,Ga)N interface. The corresponding images of the interface between the GaN core top facet and the (Al,Ga)N cap as well as of the GaN core side facet and the (Al,Ga)N shell recorded along the <11$\bar{2}$0> zone axis are displayed in Fig. 6b and c, respectively. The brighter areas correspond to the GaN core whereas the dark gray regions belong to the (Al,Ga)N cap and shell. For both materials, the

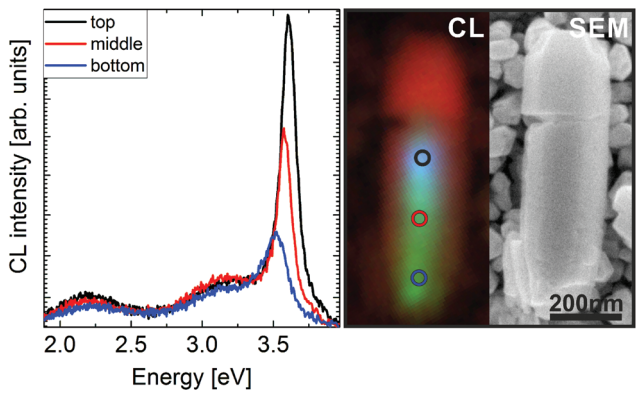

Fig. 5 Room temperature CL spectra of distinct sites along a cone-shaped GaN–(Al,Ga)N core–shell NW grown on Si with corresponding false-colored CL map and SEM image of the NW.

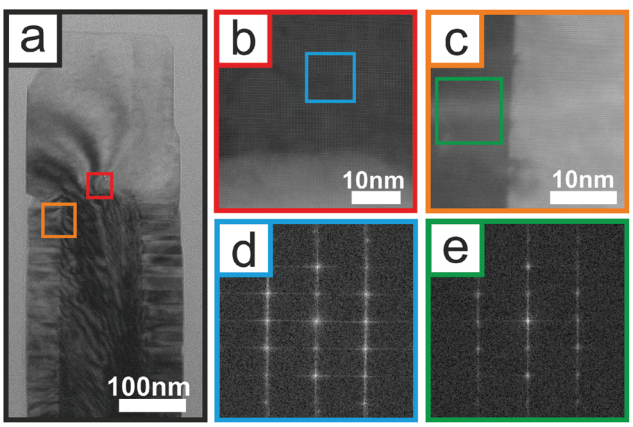

Fig. 6 (a) Cross-sectional TEM image of the upper part of a GaN–(Al,Ga)N core–shell NW grown on Si. HAADF STEM images of (b) the GaN core/(Al,Ga)N cap interface (red square in (a)) and (c) the GaN core/(Al,Ga)N shell interface (orange square in (a)). FFT patterns of (d) the (Al,Ga)N cap (blue square in (b)) and (e) the (Al,Ga)N shell (green square in (c)).

characteristic ABAB stacking sequence of the wurtzite crystal structure has been identified. Moreover, local variations of the contrast could be either a distortion of the crystal or artifacts arising from the lamella fabrication, *e.g.*, an inhomogeneous ablation of the shell. Note that these effects are also responsible for the limited resolution of the obtained images and for the observation of small GaN-free cracks at the side facets of the GaN/(Al,Ga)N interface (Fig. 6c). Since these extended defects in the GaN core have not been observed in TEM measurements on untreated core–shell NWs, we assign this to a damaging of the GaN core by the FIB preparation.

A key requirement for building up high strain fields in the GaN core is that the (Al,Ga)N shell is free of defect-related strain relaxation. Thus, a single crystalline growth perpendicular to the NW growth axis is obligatory to distribute the elastic energy over the whole thickness of the shell and to exert a maximum force on the GaN core.[9,36] To determine the crystal quality of the (Al,Ga)N in an appropriate way the Fast Fourier Transform (FFT) patterns of two distinct regions, namely the cap (Fig. 6b) and the shell (Fig. 6c) are illustrated in Fig. 6d and e, respectively. Both FFT patterns show the typical wurtzite pattern.[18] However, a clear broadening in both directions, *i.e.* parallel and perpendicular to the NW axis, can be observed in the case of the cap whereas for the shell a broadening only appears parallel to the NW axis. A smearing of the spots of the FFT patterns is equivalent to a decrease of the coherence length of the crystal, *i.e.* its periodicity and is, thus, a measure for the structural crystal quality. Consequently, it can be concluded that the (Al,Ga)N crystal of the shell is of superior quality compared to that of the cap.

The uniaxial broadening in the case of the shell (Fig. 6e) is manifested by the crystallite growth which could only been visualized in TEM (Fig. 6a) but not in HAADF STEM (Fig. 6b). The respective crystallites are thus expected to be single crystalline over the whole shell thickness. Possible origins for this kind of crystal appearance could be the lattice mismatch or the different thermal expansion coefficients of GaN and (Al,Ga)N, which can induce defects or cracks, respectively.[8,37] As the thermal expansion of the AlN and GaN crystal lattices differ only by 0.17% for $\Delta T \approx 800$ K, a crack formation during cooldown is not believed to be the reason.[38] In contrast, the lattice mismatch between GaN and (Al,Ga)N is ≈3.9% for an Al content of 95%. Assuming lattice mismatch-induced defects at the interface between the (Al,Ga)N crystallites, this could lead to a partial relaxation of strain. Hestroffer *et al.* have observed edge type dislocations introducing an additional AlN *c*-plane on GaN–AlN core–shell NWs.[8] If this would be the same in the present study, a defect spacing of 20–30 nm (Fig. 6a) would lead to 2–3% relaxation. However, in a previous work, the occurring strain within the GaN core has been measured by means of PL and Raman spectroscopy and compared to numerical simulations of an ideal core–shell strain system, without assuming any relaxation effects.[4] As a result, the theoretically obtained values coincide well with the experimental data, which indicates a subordinate role of possible defects within the shell on the overall strain state. Thus, edge type dislocations cannot be the origin for the observed crystallite growth. In contrast, the particular appearance of the (Al,Ga)N shell might be the result of a complex nucleation behavior of the shell, which will be further addressed below.

The biaxial broadening of the spots of the FFT pattern for the cap (Fig. 6d) agrees with the higher BL defect luminescence observed in CL (Fig. 3b), which has been attributed to a higher density of Al vacancies within the crystal lattice. In addition, stacking faults within the cap could be a reason for the smearing of the spots in particular in *c*-direction.[39]

The site-dependent crystal characteristics of (Al,Ga)N grown on SAG GaN NWs implies a complex nucleation behavior of the shell. To further address this, a series of GaN–(Al,Ga)N core–shell NWs with varying t_{shell} has been grown on Si. In Fig. 7, 45°-tilted view SEM images of SAG GaN–(Al,Ga)N core–shell NWs with 0′, 3′, 9′ and 30′ deposition time of the shell and a fixed core diameter of ≈40 nm are depicted. Bare GaN NWs (t_{shell} = 0′) exhibit the well-known straight-lined orientation with a uniform growth direction of the respective crystals. However, after 3′ of shell growth, some NWs adopt a curvy shape with no clear trend in a distinct direction. This effect increases with decreasing core diameter. After 9′ growth, most of the NWs are again straight, whereas a small amount still shows a slight curviness. Thus, the bowing of the core–shell NWs seems to reach its largest extent directly after nucleation and, subsequently, a straightening occurs. Finally, for 30′ growth and shell thicknesses of ≈50 nm all core–shell NWs show a straight shape and a full disappearance of the observed bowing. Mohan *et al.* have observed bending of InP–InAs core–shell NWs with a shell thickness of ≈10 nm and proposed a partly exposed core in combination with built-in strain to be the reason for this effect.[40] To clarify this for the present material system, NWs with a small core diameter and a shell nucleation time of 3′ have been imaged by TEM. For comparison, bare SAG GaN NWs have also been investigated. For this study, the NWs have been released from their original substrate, whereas no thinning has been done to preclude any perturbation of the strain state.

In Fig. 8a, a cross-sectional TEM image of a SAG GaN NW released from a Si (111) substrate is displayed. The right upper region corresponds to the NW top facet. After a nucleation phase of about 30 nm where tapering out of the TiN mask

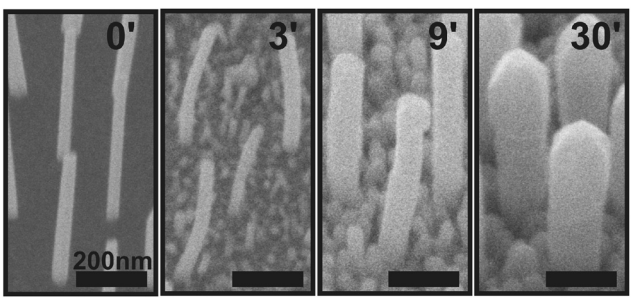

Fig. 7 Tilted view SEM images (45°) of GaN–(Al,Ga)N core–shell NWs on Si for different growth times of the shell.

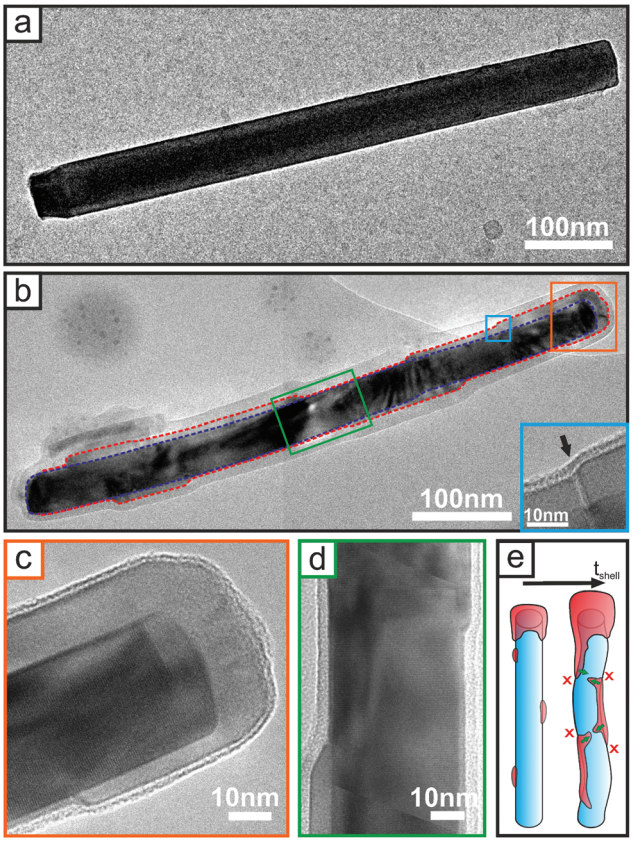

Fig. 8 Cross-sectional TEM image of (a) a bare SAG GaN NW grown on Si and (b) a SAG GaN–(Al,Ga)N core–shell NW after 3′ shell growth. The GaN core and the (Al,Ga)N shell are indicated with dashed lines as a guide to the eye. The outer shading surrounding this NW is assigned to contamination. High magnification image of (c) the core–shell cap and (d) a distinct location along the NW side facets of (b). The magnified areas are indicated with an orange and green box in (b), respectively. (e) Schematic sketch of the proposed shell nucleation process with the GaN core in blue and the (Al,Ga)N shell in red color. The red crosses and the green arrows indicate hindered and preferred growth directions of the shell, respectively.

hole occurs, the NW exhibits a constant diameter over the whole length. In addition, no extended defects such as cracks or misorientated nucleation can be observed, neither within the bulk nor along the sidewalls. In contrast, a core–shell NW with 3′ (Al,Ga)N shell growth and a core diameter of 40 nm is depicted in Fig. 8b. To better distinguish between the GaN core and the (Al,Ga)N shell, blue and red dashed lines indicating the respective outer interfaces are inserted as a guide to the eye. Note that the occurring shading around the NW is attributed to a contamination caused by the NW releasing step. Obviously, distinct inhomogeneities of the shell nucleation are present after this short growth time. In particular, a significant growth on the top facet takes place (Fig. 8c), whereas nucleation spots along the side facets seem to be arbitrarily distributed. In addition, the NW is bent in different directions at different positions along the NW (Fig. 8b). This bending correlates with the position of extended (Al,Ga)N nuclei on the sidewalls. Naturally, this can be explained by an asymmetrical strain acting on the GaN core where a higher compression occurs at the larger (Al,Ga)N shell side, leading to the observed bowing. Note that no cracks have been observed within the GaN core for all NWs investigated which is in contrast to the STEM measurements in Fig. 6b. This supports the attribution of cracks in Fig. 6b to artifacts arising from the FIB thinning of the NW.

However, structural defects have been observed within the (Al,Ga)N shell (Fig. 8b inset). These kind of defects have been found along the whole NW, with arbitrary distances of several tens of nanometers to each other. In some cases, the shell thickness changes at the position of such a defect, which indicates grain boundaries between different shell nuclei to be the reason for this. In addition, this can explain the crystallite appearance of the shell observed in TEM measurements on core–shell NWs with thicker shells (Fig. 6a). Assuming a locally increased density of these defects at a certain position along the NW, this might cause a partial relaxation of strain at this place, which explains the local redshift of ≈20 meV observed in CL measurements (Fig. 3b).

To understand this complex nucleation behavior of the shell along the GaN sidewalls, a high resolution TEM image of a distinct region along the NW side facet is shown in Fig. 8d. Note that the diagonal lines crossing the NW at the top and the bottom of the image are artifacts of the image processing. At the bottom left as well as at the upper right side of the NW, distinct (Al,Ga)N shell growth occurs with a thickness of 6.5 and 4.5 nm, respectively, in this particular case. However, a sudden decrease of the shell thickness within a transition zone of 4.5 to 9 nm parallel to the NW axis can be observed. Then, only some monolayers of (Al,Ga)N with an average thickness of ≈1.5 nm remain along the GaN core. Interestingly, it has been observed on numerous NWs investigated that the nucleation spots of these thicker (Al,Ga)N crystallites switch to the opposite side with either no or only several tens of nanometers overlap on both sides (Fig. 8d). Thus, we assume that the different (Al,Ga)N nuclei can affect each other during the nucleation phase. Moreover, TEM images on thicker GaN cores but for equivalent shell growth times reveal a decreased maximum thickness and a larger extent along the NW axis of the (Al,Ga)N nuclei. This indicates that the shell growth rate decreases, whereas its homogeneity increases for thicker GaN cores. In addition, for larger core diameters, a significant amount of flaked off shell nuclei have been observed in the vicinity of the dispersed NWs. This can be assigned to a higher strain acting on the shell and, thus, leading to a cracking of the respective crystals during mechanical lift off of the NWs from their original substrate. The corresponding TEM images of core–shell NWs with a thicker GaN core and additional examples for thin cores can be found in the ESI.† In addition, CL measurements have been performed on GaN–(Al,Ga)N core–shell NWs with a thin shell of 10–15 nm thickness (ESI†). Similar to the measurements on a cone-shaped NW (Fig. 5), an intensity quenching of X_C has been observed for an asymmetric strain profile, whereas the defect luminescence remains unaffected.

Based on these observations a strain-driven nucleation model of the (Al,Ga)N shell is proposed and discussed in the following. First, (Al,Ga)N nucleation occurs at the GaN NW top facet since growth in *c*-direction is favorable for wurtzite NW crystals.[41] However, after a short time interval, arbitrarily distributed nucleation spots start to appear along the NW sidewalls as well. Possible reasons for a preferential shell nucleation site could be defects, dislocations or atomic steps at the GaN NW sidewalls,[8] or a local accumulation of supplied metal atoms from the effusion cells. A schematic sketch of the nucleation phase of the separated shell crystallites is illustrated in Fig. 8e (left NW). Due to a local compression of the GaN beneath the (Al,Ga)N nuclei, a bowing of the NWs sets in at these sites. This, in turn, reduces the local lattice parameters which makes (Al,Ga)N growth even more preferential in this region so that the nuclei are able to expand laterally as well as in their thickness (Fig. 8e, right NW). This growth continues in the energetically favored *c*-direction until an (Al,Ga)N nucleus, located on the opposite side of the NW, is reached. Due to the compression of the GaN on the one side of the NW, this induces an increase of the lattice parameters on the opposite side and, thus, effectively hinders further (Al,Ga)N nucleation at this place (marked with red crosses in Fig. 8e). As a consequence, the shell growth proceeds along the direction of best nucleation conditions, *i.e.* smallest lattice parameters, which is (in this case) the lateral crossing of the GaN NW toward the opposite side (marked with green arrows in Fig. 8e) so that coalescence of separated nuclei occurs after a distinct growth time. This self-regulating nucleation behavior, eventually, leads to a dense shell with a constant thickness and a homogeneous strain level within the GaN–(Al,Ga)N core–shell NW heterostructure. Thus, after an inhomogeneous nucleation stage, the (Al,Ga)N shell repairs itself for a sufficiently long growth time.

4. Conclusions

We have investigated the structural and optical characteristics of heteroepitaxial selective area-grown GaN–(Al–Ga)N core–shell nanowire heterostructures on the nanoscale and have addressed the growth behavior of the shell during the nucleation stage. In particular, GaN–(Al,Ga)N core–shell nanowire arrays with different shell geometries and substrate species have been compared. Photoluminescence measurements show an energy variation of the emitted light due to strain and a decrease of the photoluminescence intensity by two orders of magnitude compared to bare GaN nanowires. However, this intensity quenching is a substrate-specific effect which appears on Si (111) but not on diamond (111) substrates. Thus, we assume Si-related defect centers at the GaN/(Al,Ga)N interface to be responsible for this. This is further verified by power-dependent photoluminescence measurements which indicate defect saturation in the case of core–shell NWs on Si. Cathodoluminescence measurements on a GaN nanowire and a GaN–(Al,Ga)N core–shell nanowire complement macroscopic photoluminescence measurements and prove a high homogeneity of the luminescence within both the GaN core and the (Al,Ga)N shell. A higher defect luminescence of the (Al,Ga)N cap indicates a reduced crystal quality compared to the lateral shell growth along the side facets. This is substantiated by scanning transmission electron microscopy on equivalent core–shell nanowires. Moreover, there is evidence suggesting that yellow luminescence arising from the GaN nanowire surface is effectively attenuated thanks to passivation with the (Al,Ga)N shell. The presence of a strain gradient due to an intentional variation of the shell thickness along a core–shell NW results in a local quenching of the luminescence intensity toward the lower strain region. To obtain knowledge of the (Al,Ga)N shell nucleation process, a shell growth time series has been investigated. After a short deposition time of 3′ the nanowires show a pronounced random bending along the *c*-direction. This bending disappears again for ongoing shell growth until a full re-alignment is accomplished. A transmission electron microscopy study on bent nanowires reveals the nucleation of separated (Al,Ga)N islands which locally compress the GaN core and lead to the observed nanowire bending. A detailed study of the shell nucleation process suggests a strain-based self-regulating (Al,Ga)N shell nucleation mechanism.

Acknowledgements

Financial support from the Deutsche Forschungsgemeinschaft (DFG) *via* the Forschergruppe 1493, TUM.solar in the frame of the Bavarian Collaborative Research Project "Solar technologies go Hybrid" (SolTec), the excellence cluster Nanosystems Initiative Munich (NIM) and the Fonds National Suisse de la Recherche Scientifique (FNS) through the National Centre of Competence in Research (NCCR) "QSIT – Quantum Science and Technology" is gratefully acknowledged. Further we thank the Centre Interdisciplinaire de Microscopie Électronique (CIME) for the access to the CL microscope.

References

1 S. Albert, A. Bengoechea-Encabo, J. Ledig, T. Schimpke, M. A. Sánchez-Garcia, M. Strassburg, A. Waag and E. Calleja, *Cryst. Growth Des.*, 2015, **15**, 3661–3665.
2 T. Schimpke, H.-J. Lugauer, A. Avramescu, T. Varghese, A. Koller, J. Hartmann, J. Ledig, A. Waag and M. Strassburg, *Proc. SPIE*, 2016, **9768**, 97680T–97680T.
3 H. Zhang, X. Dai, N. Guan, A. Messanvi, V. Neplokh, V. Piazza, M. Vallo, C. Bougerol, F. H. Julien, A. Babichev, N. Cavassilas, M. Bescond, F. Michelini, M. Foldyna, E. Gautier, C. Durand, J. Eymery and M. Tchernycheva, *ACS Appl. Mater. Interfaces*, 2016, **8**, 26198–26206.
4 M. Hetzl, M. Kraut, J. Winnerl, L. Francaviglia, M. Döblinger, S. Matich, A. Fontcuberta i Morral and M. Stutzmann, *Nano Lett.*, 2016, **16**, 7098–7106.

5 H. Sekiguchi, K. Kishino and A. Kikuchi, *Appl. Phys. Express*, 2008, **1**, 124002.
6 K. Kishino, T. Hoshino, S. Ishizawa and A. Kikuchi, *Electron. Lett.*, 2008, **44**, 819–821.
7 F. Schuster, M. Hetzl, S. Weiszer, J. A. Garrido, M. de la Mata, C. Magen, J. Arbiol and M. Stutzmann, *Nano Lett.*, 2015, **15**, 1773.
8 K. Hestroffer, R. Mata, D. Camacho, C. Leclere, G. Tourbot, Y. M. Niquet, A. Cros, C. Bougerol, H. Renevier and B. Daudin, *Nanotechnology*, 2010, **21**, 415702.
9 L. Rigutti, G. Jacopin, L. Largeau, E. Galopin, A. De Luna Bugallo, F. H. Julien, J.-C. Harmand, F. Glas and M. Tchernycheva, *Phys. Rev. B: Condens. Matter*, 2011, **83**, 155320.
10 G. Jacopin, L. Rigutti, S. Bellei, P. Lavenus, F. H. Julien, A. V. Davydov, D. Tsvetkov, K. A. Bertness, N. A. Sanford, J. B. Schlager and M. Tchernycheva, *Nanotechnology*, 2012, **23**, 325701.
11 P. Stepanov, M. Elzo-Aizarna, J. Bleuse, N. S. Malik, Y. Curé, E. Gautier, V. Favre-Nicolin, J.-M. Gérard and J. Claudon, *Nano Lett.*, 2016, **16**, 3215–3220.
12 J. Pastrnák and L. Roskovcová, *Phys. Status Solidi. B*, 1966, **14**, K5–K8.
13 P. Lefebvre, S. Albert, J. Ristić, S. Fernández-Garrido, J. Grandal, M.-A. Sánchez-García and E. Calleja, *Superlattices Microstruct.*, 2012, **52**, 165–171.
14 C. Pfüller, O. Brandt, F. Grosse, T. Flissikowski, C. Chèze, V. Consonni, L. Geelhaar, H. T. Grahn and H. Riechert, *Phys. Rev. B: Condens. Matter*, 2010, **82**, 045320.
15 J. Teubert, P. Becker, F. Furtmayr and M. Eickhoff, *Nanotechnology*, 2011, **22**, 275505.
16 R. A. Youngman and J. H. Harris, *J. Am. Ceram. Soc.*, 1990, **73**, 3238–3246.
17 F. Furtmayr, M. Vielemeyer, M. Stutzmann, J. Arbiol, S. Estradé, F. Peirò, J. R. Morante and M. Eickhoff, *J. Appl. Phys.*, 2008, **104**, 034309.
18 F. Schuster, F. Furtmayr, R. Zamani, C. Magén, J. R. Morante, J. Arbiol, J. A. Garrido and M. Stutzmann, *Nano Lett.*, 2012, **12**, 2199.
19 M. Hetzl, F. Schuster, A. Winnerl, S. Weiszer and M. Stutzmann, *Mater. Sci. Semicond. Process.*, 2016, **48**, 65–78.
20 F. Schuster, A. Winnerl, S. Weiszer, M. Hetzl, J. A. Garrido and M. Stutzmann, *J. Appl. Phys.*, 2015, **117**, 044307.
21 L. Yang, J. Motohisa, K. Tomioka, J. Takeda, T. Fukui, M. M. Geng, L. X. Jia, L. Zhang and Y. L. Liu, *Nanotechnology*, 2008, **19**, 275304.
22 M. A. Zimmler, J. Bao, F. Capasso, S. Müller and C. Ronning, *Appl. Phys. Lett.*, 2008, **93**, 051101.
23 E. C. Le Ru, J. Fack and R. Murray, *Phys. Rev. B: Condens. Matter*, 2003, **67**, 245318.
24 G. D. Chen, M. Smith, J. Y. Lin, H. X. Jiang, S. Wei, M. Asif Khan and C. J. Sun, *Appl. Phys. Lett.*, 1996, **68**, 2784–2786.
25 J. Neugebauer and C. G. Van de Walle, *Appl. Phys. Lett.*, 1996, **69**, 503–505.
26 T. Suski, P. Perlin, H. Teisseyre, M. Leszczyński, I. Grzegory, J. Jun, M. Boćkowski, S. Porowski and T. D. Moustakas, *Appl. Phys. Lett.*, 1995, **67**, 2188–2190.
27 J. L. Lyons, A. Janotti and C. G. Van de Walle, *Appl. Phys. Lett.*, 2010, **97**, 152108.
28 T. Ogino and M. Aoki, *Jpn. J. Appl. Phys.*, 1980, **19**, 2395.
29 Q. Li and G. T. Wang, *Nano Lett.*, 2010, **10**, 1554–1558.
30 S.-C. Shi, C. F. Chen, S. Chattopadhyay, K.-H. Chen, B.-W. Ke, L.-C. Chen, L. Trinkler and B. Berzina, *Appl. Phys. Lett.*, 2006, **89**, 163127.
31 K. B. Nam, M. L. Nakarmi, J. Y. Lin and H. X. Jiang, *Appl. Phys. Lett.*, 2005, **86**, 222108.
32 E. Monroy, J. Zenneck, G. Cherkashinin, O. Ambacher, M. Hermann, M. Stutzmann and M. Eickhoff, *Appl. Phys. Lett.*, 2006, **88**, 071906.
33 B. N. Pantha, A. Sedhain, J. Li, J. Y. Lin and H. X. Jiang, *Appl. Phys. Lett.*, 2010, **96**, 131906.
34 S. J. Henley and D. Cherns, *J. Appl. Phys.*, 2003, **93**, 3934–3939.
35 X. Zhang, D. H. Rich, J. T. Kobayashi, N. P. Kobayashi and P. D. Dapkus, *Appl. Phys. Lett.*, 1998, **73**, 1430–1432.
36 S. Raychaudhuri and E. T. Yu, *J. Appl. Phys.*, 2006, **99**, 114308.
37 S. Conesa-Boj, H. I. T. Hauge, M. A. Verheijen, S. Assali, A. Li, E. P. A. M. Bakkers and A. Fontcuberta i Morral, *Nano Lett.*, 2015, **15**, 2974–2979.
38 S. Strite and H. Morkoç, *J. Vac. Sci. Technol., B*, 1992, **10**, 1237–1266.
39 D. Poppitz, A. Lotnyk, J. W. Gerlach, J. Lenzner, M. Grundmann and B. Rauschenbach, *Micron*, 2015, **73**, 1–8.
40 P. Mohan, J. Motohisa and T. Fukui, *Appl. Phys. Lett.*, 2006, **88**, 013110.
41 L. Geelhaar, C. Chèze, B. Jenichen, O. Brandt, C. Pfüller, S. Münch, R. Rothemund, S. Reitzenstein, A. Forchel, T. Kehagias, P. Komninou, G. P. Dimitrakopulos, T. Karakostas, L. Lari, P. R. Chalker, M. H. Gass and H. Riechert, *IEEE J. Sel. Top. Quantum Electron*, 2011, **17**, 878–888.

